

Part I

Low-Scale Technicolor at the LHC

*G. Azuelos, K. Black, T. Bose, J. Ferland
Y. Gershtein, K. Lane and A. Martin*

Abstract

If technicolor is responsible for electroweak symmetry breaking, there are strong phenomenological arguments that its energy scale is at most a few hundred GeV and that the lightest technihadrons are within reach of the ATLAS and CMS experiments at the LHC. Furthermore, the spin-one technihadrons ρ_T , ω_T and a_T are expected to be very narrow, with striking experimental signatures involving decays to pairs of electroweak gauge bosons (γ , W , Z) or an electroweak boson plus a spin-zero π_T . Preliminary studies of signals and backgrounds for such modes are presented. With luminosities of a few to a few tens of femtobarns, almost all the spin-one states may be discovered up to masses of about 600 GeV. With higher luminosities, one can observe decay angular distributions and technipions that establish the underlying technicolor origin of the signals. Preliminary ATLAS studies show that, with 50–100 fb⁻¹ and assuming $M_{a_T} \simeq 1.1M_{\rho_T}$, both processes $\rho_T^\pm, a_T^\pm \rightarrow Z^0 W^\pm$ (with $M_{\rho_T} \simeq 500$ GeV) may be seen in the $\ell^+ \ell^- \ell^\pm \nu_\ell$ final state and $\rho_T^\pm, a_T^\pm \rightarrow Z^0 \pi_T^\pm$ (up to $M_{\rho_T} \simeq 400$ GeV) in $\ell^+ \ell^- b$ jet, where $\ell = e, \mu$.

1. INTRODUCTION

Technicolor (TC) is a proposed strong gauge interaction responsible for the dynamical breakdown of electroweak symmetry [1, 2]. Modern technicolor has a slowly-running (“walking”) gauge coupling [3, 4, 5, 6]. This feature allows extended technicolor (ETC) [7] to generate realistic masses for quarks, leptons and technipions (π_T) with the very large ETC boson masses (10^3 – 10^4 TeV) necessary to suppress flavor-changing neutral current interactions. (For reviews, see Refs. [8, 9].) The important phenomenological consequence of walking is that the technicolor scale is likely to be much lower and the spectrum of this low-scale technicolor (LSTC) much richer and more experimentally accessible [10, 11, 12] than originally thought [13]. The basic argument is this: (1) The walking TC gauge coupling requires either a large number N_D of technifermion doublets so that $\Lambda_{TC} \simeq 250 \text{ GeV} / \sqrt{N_D} \lesssim 100 \text{ GeV}$, or two TC scales, one much lower than 250 GeV.¹ (2) Walking enhances π_T masses much more than those of their vector partners, ρ_T and ω_T . This effect probably closes the all- π_T decay channels of the lightest techni-vectors. In LSTC, then, we expect that the lightest ρ_T and ω_T lie below about 0.5 TeV and that they decay to an electroweak boson (γ , W , Z) plus π_T ; a pair of electroweak bosons; and $\bar{f}f$, especially $\ell^+ \ell^-$. These channels have very distinctive signatures, made all the more so because ρ_T and ω_T are very narrow, $\Gamma(\rho_T) \simeq 1$ – 5 GeV and $\Gamma(\omega_T) \simeq 0.1$ – 0.5 GeV. Technipions

¹For an alternate view based on a small TC gauge group, $SU(2)$, see Refs. [14, 15].

are expected to decay via ETC interactions to the heaviest fermion-antifermion flavors allowed kinematically, providing the best chance of their being detected.

Many higher-mass states are reasonably expected in addition to ρ_T and ω_T . In Refs. [16, 17] it was argued that walking TC invalidates the standard QCD-based calculations of the precision-electroweak S -parameter [18, 19, 20, 21]. In particular, the spectral functions appearing in S cannot be saturated by a single ρ_T and its axial-vector partner a_T . Thus, walking TC produces something like a tower of vector and axial-vector isovector states above the lightest ρ_T and a_T . All (or many) of them may contribute significantly to the S -parameter.² Most important phenomenologically, in models with small S , the lightest a_T and ρ_T likely are nearly degenerate and have similar couplings to their respective weak vector and axial-vector currents; see, e.g., Refs. [22, 23, 24, 25, 26]. The $3\pi_T$ -decay channels of the a_T are closed, so these states are also very narrow, $\Gamma(a_T) \lesssim 0.5 \text{ GeV}$.

The ρ_T , ω_T , a_T , and π_T of low-scale technicolor that we consider are bound states of the lightest technifermion electroweak doublet, (T_U, T_D) . The phenomenology of these technihadrons is set forth in the ‘‘Technicolor Straw-Man Model’’ (TCSM) [27, 28, 26]. The TCSM’s most important assumptions are: (1) There are N_D isodoublets of technifermions transforming according to the fundamental representation of the TC gauge group. The lightest doublet is an ordinary-color singlet.³ We use $N_D = 9$ in calculations; then, the technipion decay constant $F_T \simeq 246 \text{ GeV}/\sqrt{N_D} = 82 \text{ GeV}$. The technipion isotriplet composed of the lightest technifermions is a simple two-state admixture,

$$|\Pi_T^{\pm,0}\rangle = \sin \chi |W_L^{\pm,0}\rangle + \cos \chi |\pi_T^{\pm,0}\rangle, \quad (1)$$

where W_L is a *longitudinally*-polarized weak boson and π_T is a mass eigenstate, the lightest technipion referred to above, and $\sin \chi = F_T/246 \text{ GeV} = 1/\sqrt{N_D}$. This is why the lightest spin-one technihadrons are so narrow: all their decay amplitudes are suppressed by a power of $\sin \chi$ for each W_L emitted and by a power of $e = g \sin \theta_W$ for each *transversely*-polarized W_\perp . In addition, decays to π_T are phase-space limited.⁴ The technihadrons’ principal decay modes are listed in Table 1. (2) The lightest bound-state technihadrons may be treated *in isolation*, without significant mixing or other interference from higher-mass states. (3) Techni-isospin is a good symmetry.⁵ These assumptions allow the TCSM to be described by a relatively small number of parameters. The ones used for the present study are, we believe, fairly generic; they are listed below.

The main discovery channel for low-scale technicolor at the Tevatron is $\rho_T \rightarrow W^\pm \pi_T \rightarrow \ell^\pm \nu_\ell b q$, with at least one tagged b -jet. At the LHC, this channel is swamped by a $t\bar{t}$ background 100 times larger than at the Tevatron. There the discovery channels will be WZ , γW and γZ , with the weak bosons decaying into charged leptons.⁶ In the TCSM each of these modes is

²These higher mass states are also important in unitarizing longitudinal gauge boson scattering at high energies.

³Some of these doublets may be color nonsinglets with, e.g., three doublets for each color triplet. Technifermions get ‘‘hard’’ masses from ETC and ordinary color interactions and will have some hierarchy of masses. We expect that the lightest will be color-singlets.

⁴Because the interactions of the techni-vectors with electroweak gauge bosons (and fermions) are suppressed by $\sin \chi$, they can be light, $\gtrsim 200 \text{ GeV}$, without conflicting with precision electroweak and Tevatron data.

⁵Also, something like topcolor-assisted technicolor [29] is needed to keep the top quark from decaying copiously into $\pi_T^+ b$ when $M_{\pi_T} \lesssim 160 \text{ GeV}$. Thus, if π_T^+ is heavier than the top, it will not decay exclusively to $t\bar{b}$.

⁶The channel $\rho_T^\pm \rightarrow W^\pm Z^0$ was studied by P. Kreuzer, *Search for Technicolor at CMS in the $\rho_{TC} \rightarrow W + Z$ Channel*, CMS Note 2006/135, and Ref. [30]. To consider the decay angular distributions, we employ somewhat different cuts than he did.

Process	$V_{V_T/a_T G \pi_T}$	$A_{V_T/a_T G \pi_T}$
$\omega_T \rightarrow \gamma \pi_T^0$	$\cos \chi$	0
$\rightarrow \gamma Z_L^0$	$\sin \chi$	0
$\rightarrow W^\pm \pi_T^\mp$	$\cos \chi / (2 \sin \theta_W)$	0
$\rightarrow W^\pm W_L^\mp$	$\sin \chi / (2 \sin \theta_W)$	0
$\rightarrow Z^0 \pi_T^0$	$\cos \chi \cot 2\theta_W$	0
$\rightarrow Z^0 Z_L^0$	$\sin \chi \cot 2\theta_W$	0
$\rho_T^0 \rightarrow W_L^\pm \pi_T^\mp$	$\sin \chi \cos \chi$	—
$\rightarrow W_L^+ W_L^-$	$\sin^2 \chi$	—
$\rightarrow \gamma \pi_T^0$	$(Q_U + Q_D) \cos \chi$	0
$\rightarrow \gamma Z_L^0$	$(Q_U + Q_D) \sin \chi$	0
$\rightarrow W^\pm \pi_T^\mp$	0	$\pm \cos \chi / (2 \sin \theta_W)$
$\rightarrow W^\pm W_L^\mp$	0	$\pm \sin \chi / (2 \sin \theta_W)$
$\rightarrow Z^0 \pi_T^0$	$-(Q_U + Q_D) \cos \chi \tan \theta_W$	0
$\rightarrow Z^0 Z_L^0$	$-(Q_U + Q_D) \sin \chi \tan \theta_W$	0
$\rho_T^\pm \rightarrow W_L^\pm \pi_T^0$	$\sin \chi \cos \chi$	—
$\rightarrow Z_L^0 \pi_T^\pm$	$\sin \chi \cos \chi$	—
$\rightarrow W_L^\pm Z_L^0$	$\sin^2 \chi$	—
$\rightarrow \gamma \pi_T^\pm$	$(Q_U + Q_D) \cos \chi$	0
$\rightarrow \gamma W_L^\pm$	$(Q_U + Q_D) \sin \chi$	0
$\rightarrow Z^0 \pi_T^\pm$	$-(Q_U + Q_D) \cos \chi \tan \theta_W$	$\pm \cos \chi / (\sin 2\theta_W)$
$\rightarrow Z^0 W_L^\pm$	$-(Q_U + Q_D) \sin \chi \tan \theta_W$	$\pm \sin \chi / (\sin 2\theta_W)$
$\rightarrow W^\pm \pi_T^0$	0	$\mp \cos \chi / (2 \sin \theta_W)$
$\rightarrow W^\pm Z_L^0$	0	$\mp \sin \chi / (2 \sin \theta_W)$
$a_T^0 \rightarrow W^\pm \pi_T^\mp$	0	$\mp \cos \chi / (2 \sin \theta_W)$
$\rightarrow W^\pm W_L^\mp$	0	$\mp \sin \chi / (2 \sin \theta_W)$
$a_T^\pm \rightarrow \gamma \pi_T^\pm$	0	$\mp \cos \chi$
$\rightarrow \gamma W_L^\pm$	0	$\mp \sin \chi$
$\rightarrow W^\pm \pi_T^0$	0	$\pm \cos \chi / (2 \sin \theta_W)$
$\rightarrow Z^0 \pi_T^\pm$	0	$\mp \cos \chi \cot 2\theta_W$
$\rightarrow W^\pm Z_L^0$	0	$\pm \sin \chi / (2 \sin \theta_W)$
$\rightarrow W_L^\pm Z^0$	0	$\mp \sin \chi \cot 2\theta_W$

Table 1: Amplitude factors for the dominant decay modes of $\rho_T \rightarrow W_L \pi_T$, $W_L W_L$ and ρ_T , ω_T , $a_T \rightarrow G \pi_T$, $G W_L$ [28, 26]. Here, W_L is a longitudinally-polarized and $G = \gamma, W_\perp, Z_\perp$ a transversely-polarized electroweak gauge boson. Technifermion charges are $Q_U = Q_D + 1$, and $\sin \chi = F_T / 246 \text{ GeV} = 1 / \sqrt{N_D}$. Amplitudes for $W_L \pi_T$ and $W_L W_L$ are proportional to $g_{\rho_T} = \sqrt{4\pi\alpha_{\rho_T}}$, where $\alpha_{\rho_T} = 2.16(3/N_{TC})$; those for emission of a transverse gauge boson are proportional to $e = \sqrt{4\pi\alpha}$.

dominated (generally $\gtrsim 80\%$) by production of a *single* resonance:

$$\rho_T^\pm \rightarrow W^\pm Z^0, \quad a_T^\pm \rightarrow \gamma W^\pm, \quad \omega_T \rightarrow \gamma Z^0. \quad (2)$$

In Sects. 2-4, the PGS detector simulator [31] is used for our preliminary studies of these signals and their backgrounds. None of these LHC discovery modes involve observation of an actual technipion (other than the ones already observed, W_L^\pm and Z_L^0). There are other strong-interaction scenarios of electroweak symmetry breaking (e.g., so-called Higgsless models in

five dimensions [32, 33] and deconstructed models [34, 35, 36, 37]) which predict narrow vector and axial-vector resonances, but they do not decay to technipion-like objects. Therefore, observation of technipions in the final state is important for confirming LSTC as the mechanism underlying electroweak symmetry breaking. It is possible to do this at high luminosity with the decays $\rho_T^\pm, a_T^\pm \rightarrow Z^0 \pi_T^\pm \rightarrow \ell^+ \ell^- b q$. This channel also provides the interesting possibility of observing both ρ_T^\pm and a_T^\pm in the same final state. This analysis, using ATLFast [38], is summarized in Sect. 5 [39].

In addition to the discovery of narrow resonances in these channels, the angular distributions of the two-body final states in the techni-vector rest frame provide compelling evidence of their underlying technicolor origin. Because all the modes involve at least one longitudinally-polarized weak boson, the distributions are

$$\frac{d\sigma(\bar{q}q \rightarrow \rho_T^\pm \rightarrow W_L^\pm Z_L^0)}{d\cos\theta}, \quad \frac{d\sigma(\bar{q}q \rightarrow \rho_T^\pm \rightarrow \pi_T^\pm Z_L^0)}{d\cos\theta} \propto \sin^2\theta; \quad (3)$$

$$\frac{d\sigma(\bar{q}q \rightarrow a_T^\pm \rightarrow \gamma W_L^\pm)}{d\cos\theta}, \quad \frac{d\sigma(\bar{q}q \rightarrow \omega_T \rightarrow \gamma Z_L^0)}{d\cos\theta} \propto 1 + \cos^2\theta. \quad (4)$$

It is fortunate that each of the two-electroweak-boson final states is dominated by a single technihadron resonance. Otherwise, because of the resonances' expected closeness, it would likely be impossible to disentangle the different forms. Our simulations include these angular distributions.

For Les Houches, we concentrated on three TCSM mass points that cover most of the reasonable range of LSTC scales; they are listed in Table 2. In all cases, we assumed isospin symmetry, with $M_{\rho_T} = M_{\omega_T}$ and $M_{a_T} = 1.1M_{\rho_T}$; also, the ρ_T and a_T constants describing coupling to their respective weak currents were taken equal; $\sin\chi = 1/3$; $Q_U + Q_D = 1$; $N_{TC} = 4$ for the TC gauge group $SU(N_{TC})$; and $M_{V_{1,2,3}} = M_{A_{1,2,3}} = M_{\rho_T}$ for the LSTC mass parameters controlling the strength of ρ_T, ω_T, a_T decays to a transverse electroweak boson plus π_T/W_L or ρ_T/ω_T [27, 28, 26]. PYTHIA [40] has been updated to include these and other LSTC processes, according to the rules of the TCSM. The new release and its description may be found at www.hepforge.org.

The simulations presented here, especially those using the PGS detector simulator [31], are preliminary and in many respects quite superficial.⁷ E.g., no attempt was made to optimize S/B in the PGS studies. Nor did we carry out a serious analysis of statistical, let alone systematic, errors.⁸ Still, we believe the simulations establish the LHC's ability to discover, or rule out, important signatures of low-scale technicolor. Beyond that, it is our intent that the present studies will stimulate more thorough ones by ourselves and by the ATLAS and CMS collaborations.

⁷All PGS simulations were done using the ATLAS parameter set provided with the PGS extension of MADGRAPHv4.0 [41, 42]. The relevant parameters are: calorimeter segmentation $\Delta\eta \times \Delta\phi = 0.1 \times 0.1$, jet resolution $\Delta E/E = 0.8/\sqrt{E}$, and electromagnetic resolution $\Delta E/E = 0.1/\sqrt{E} + 0.01$. To model muons more realistically, we changed the sagitta resolution to $50\mu m$. With this set of parameters, the PGS lepton identification efficiency is $\approx 90\%$ in their kinematic region of interest, $p_T > 10$ GeV and $|\eta| < 2.5$.

⁸Potentially important sources of systematic error are the higher-order QCD corrections to signal and backgrounds. The K -factors can be quite large, ~ 1.5 .

Case	$M_{\rho_T} = M_{\omega_T}$	M_{a_T}	M_{π_T}	$M_{\pi_T^{0'}}$	$\sigma(W^\pm Z^0)$	$\sigma(\gamma W^\pm)$	$\sigma(\gamma Z^0)$	$\sigma(Z^0 \pi_T^\pm)$
A	300	330	200	400	110	168	19.2	158
B	400	440	275	500	36.2	64.7	6.2	88.6
C	500	550	350	600	16.0	30.7	2.8	45.4

Table 2: Masses (in GeV) and signal cross sections (in fb) for the lightest technihadrons for the three TCSM mass points in this study. Isospin symmetry is assumed. The $\pi_T^{0'}$ is an isosinglet, color-singlet technipion expected in TC models; we have assumed it so heavy that the ρ_T , ω_T and a_T cannot decay to it. The cross sections combine contributions from ρ_T , ω_T and a_T , but tend to be dominated by a single resonance. Branching ratios of the W and Z to electrons and muons are included in all cross sections.

Background	Cross section (fb)	Comments
$WZ \rightarrow 3\ell + \nu$	429	
$ZZ \rightarrow 4\ell$	52	
$Z + bb \rightarrow \ell^+ \ell^- bb$	7600	$p_T(b) > 15.0$ GeV, $ \eta_b < 3.5$
$t\bar{t} \rightarrow 2\ell 2\nu bb$	22,800	PYTHIA generator
$W\gamma \rightarrow \ell\nu\gamma$	2560	$p_T(\gamma) > 40$ GeV, $ \eta_\gamma < 3.5$
$W \text{ jet} \rightarrow \ell\nu\gamma$ (fake)	3180	$p_T(\text{jet}) > 40$ GeV, $ \eta_{\text{jet}} < 3.5$ Includes 0.1% fake rate
$Z\gamma \rightarrow \ell^+ \ell^- \gamma$	700	$p_T(\gamma) > 40$ GeV, $ \eta_\gamma < 3.5$
$Z \text{ jet} \rightarrow \ell^+ \ell^- \gamma$ (fake)	315	$p_T(\text{jet}) > 40$ GeV, $ \eta_{\text{jet}} < 3.5$ Includes 0.1% fake rate

Table 3: Backgrounds to the $W^\pm Z^0$, γW^\pm and γZ^0 signals of low-scale technicolor. The generator is ALPGENv13 [43] unless indicated otherwise. Branching ratios of the W and Z to electrons and muons are included in the cross sections.

2. $\rho_T^\pm \rightarrow W_L^\pm Z_L^0 \rightarrow \ell^\pm \nu_\ell \ell^+ \ell^-$

The cross sections for $\rho_T^\pm \rightarrow W_L^\pm Z_L^0$, including branching ratios to electrons and muons, are listed in Table 2.⁹ Signal events were generated with the updated PYTHIA [40]. The principal backgrounds are in Table 3, along with their generators and parton-level cuts. The ALPGEN backgrounds were passed through PYTHIA for showering and hadronization.

Events were selected which have exactly three leptons, electrons and/or muons, with two having the same flavor and opposite sign, $|\eta_\ell| < 2.5$, at least one having $p_T > 30$ GeV, and the others with $p_T > 10$ GeV. No cut on \cancel{E}_T was applied in this analysis, though it may improve S/B to do so. The Z was reconstructed from two same-flavor, opposite-sign leptons with the smallest $|M_{\ell^+ \ell^-} - M_Z| < 7.8$ GeV. In reconstructing the W , $\vec{p}_T(\nu) = -\sum \vec{E}_T$ was assumed, and the quadratic ambiguity in $p_z(\nu)$ was resolved in favor of the solution minimizing the opening angle between the neutrino and the charged lepton assigned to the W , as would be expected for a boosted W .¹⁰

⁹For the TCSM parameters we use, about 20% of these $\rho_T^\pm \rightarrow W^\pm Z^0$ rates involve one transverse gauge boson.

¹⁰The efficacy of this procedure, which was adopted at Les Houches (“the LH algorithm”) was compared to a “TeV algorithm” used at the Tevatron. The TeV algorithm chooses the $p_z(\nu)$ solution which gives the smaller W energy. In ATLAS [44] and CMS-based analyses [45], it was found that the TeV algorithm does slightly better at

Figure 1 shows various distributions for case A with $p_T(W), p_T(Z) > 50$ GeV and $H_T(\text{jets}) \equiv \sum E_T(\text{jet}) < 125$ GeV. The H_T cut significantly reduces the $\bar{t}t$ background. The integrated luminosity is 10 fb^{-1} , and a strong signal peak is clearly visible above background in the first panel. Fitting the peak to a Gaussian, its mass is 311 GeV. Counting signal and background within twice the fitted resolution of 25 GeV, only $\int \mathcal{L} dt = 2.4 \text{ fb}^{-1}$ is required for a $S/\sqrt{S+B} = 5\sigma$ discovery of this resonance. Table 4 contains the final-state mass resolutions and 5σ discovery luminosities for the two-electroweak-boson modes considered here. The poorer resolution in the WZ and γW channels is due to the \cancel{E}_T resolution.¹¹

WZ	M_{peak} (GeV)	σ (GeV)	\mathcal{L}_{min} (fb^{-1})	p_T cut
A	311	25.6	2.4	$p_T(W, Z) > 50$ GeV
B	414	34.5	7.2	$p_T(W, Z) > 75$ GeV
C	515	41.0	14.7	$p_T(W, Z) > 75$ GeV
γW	M_{peak} (GeV)	σ (GeV)	\mathcal{L}_{min} (fb^{-1})	p_T cut
A	328	31.2	2.3	$p_T(\gamma, W) > 75$ GeV
B	439	39.1	4.5	$p_T(\gamma, W) > 100$ GeV
C	547	39.3	7.8	$p_T(\gamma, W) > 125$ GeV
γZ	M_{peak} (GeV)	σ (GeV)	\mathcal{L}_{min} (fb^{-1})	p_T cut
A	299	7.3	16.8	$p_T(\gamma, Z) > 80$ GeV
B	398	9.4	45.5	$p_T(\gamma, Z) > 110$ GeV
C	498	12.0	97.2	$p_T(\gamma, Z) > 150$ GeV

Table 4: PGS simulation data for the spin-one technihadrons decaying to a pair of electroweak gauge bosons. A simple Gaussian fit is made to determine the mass and width of the resonance; signal and background events are counted within $\pm 2\sigma$ of the peak value to determine the minimum luminosity needed for $S/\sqrt{S+B} = 5\sigma$.

The second panel in Fig. 1 shows the total and signal WZ angular ($|\cos\theta|$) distribution. The distribution is folded since the signal and WZ background are even functions of $\cos\theta$. The total distribution reflects the forward-backward peaking of the standard WZ production. The signal distribution (open black histogram) is much flatter than the expected $\sin^2\theta$, presumably because of poorly-fit W 's and their effect on determining M_{WZ} and the WZ rest frame. To remedy this, we take advantage of the LSTC technihadrons' very small widths and require $280 < M_{WZ} < 340$ GeV; see Fig. 2. The signal distribution now has the expected $\sin^2\theta$ shape. The remaining large background at $|\cos\theta| \gtrsim 0.7$ can be fit and subtracted by measuring the angular distribution in the sidebands $220 \lesssim M_{WZ} \lesssim 280$ GeV and $340 \lesssim M_{WZ} \lesssim 400$ GeV. We believe that 10 fb^{-1} is sufficient to distinguish this angular distribution from $1 + \cos^2\theta$, but detailed fitting is required to confirm this; see Ref. [44].

The $|\cos\theta|$ distribution in the ρ_T -resonance region is shown in Fig. 3 for cases B ($M_{\rho_T} = 400$ GeV) and C (500 GeV). The $p_T(W, Z)$ cuts of 75 and 100 GeV were chosen to accept signal choosing the correct solution.

¹¹The p_T cuts listed in this table were not optimized for discovery; rather they were chosen partly to reveal as much of the angular distributions as possible consistent with background reduction. Presumably, in a real search, harder cuts would be employed to reveal the signal. Once it was found, the p_T cut could be loosened and the final-state mass cut tightened to focus on the angular distribution. The upward shift of the ρ_T^\pm peak mass, evident in their non-Gaussian high-mass tails, may be due to $a_T^\pm \rightarrow W^\pm Z^0$ at about 20% the strength of ρ_T^\pm . These issues are being considered with more sophistication using ATLFast [38] and CMS Fast Simulation (<https://twiki.cern.ch/twiki/bin/view/CMS/WorkBookFastSimulation>) in Refs. [44, 45]. They find discovery luminosities about 15–30% lower than estimated here.

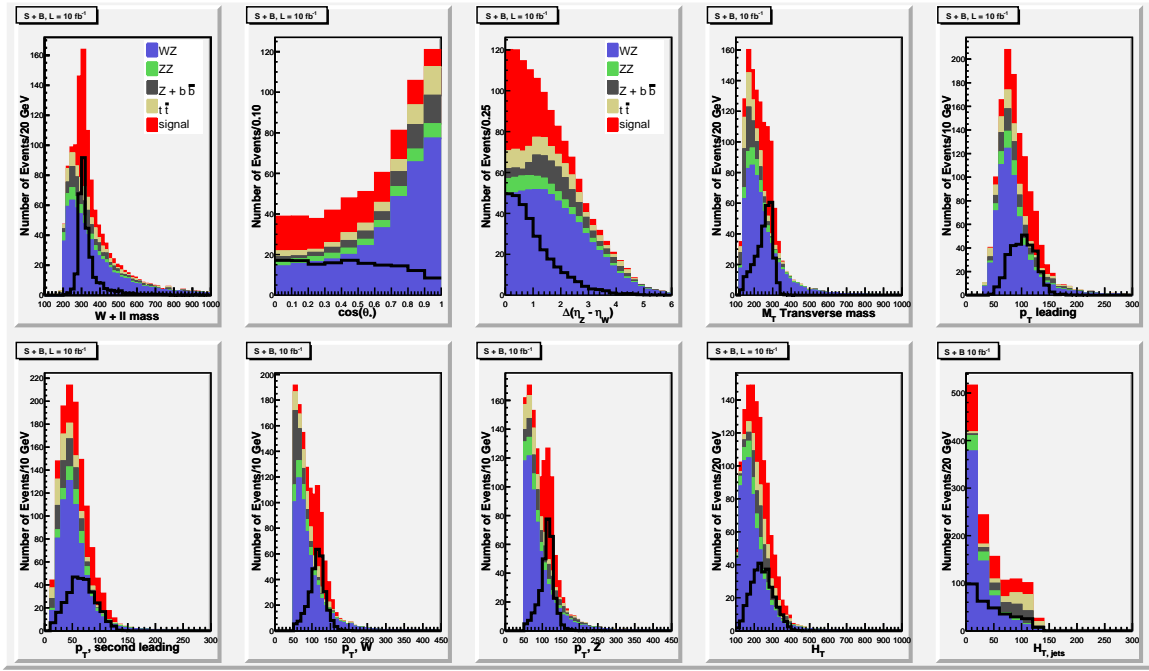


Fig. 1: Signal and background distributions of a 300 GeV $\rho_T^\pm \rightarrow W^\pm Z^0 \rightarrow \ell^\pm \nu_\ell \ell^+ \ell^-$ for 10 fb^{-1} at the LHC; $p_T(W, Z) > 50 \text{ GeV}$ and $H_T(\text{jets}) < 125 \text{ GeV}$. The open black histograms are the signal contributions.

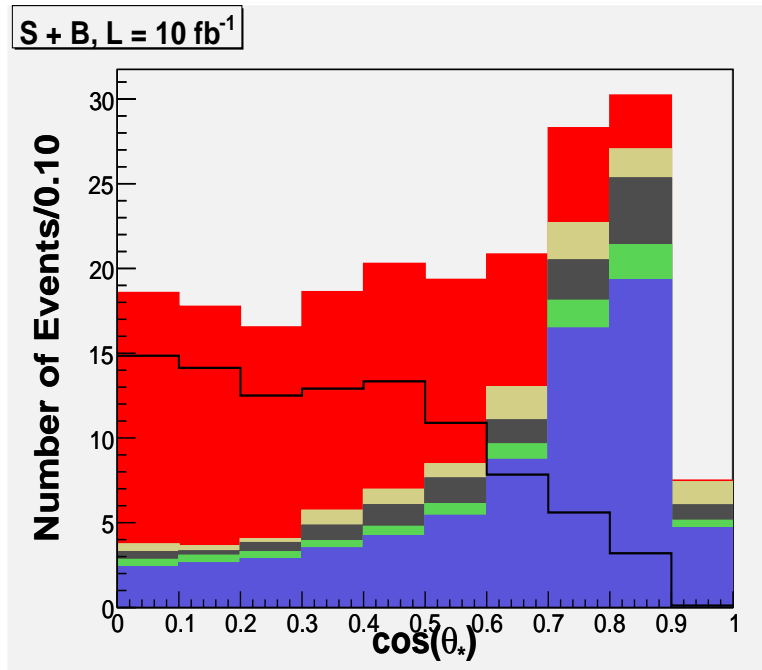


Fig. 2: WZ angular distribution of the signal and backgrounds for a 300 GeV $\rho_T^\pm \rightarrow W^\pm Z^0 \rightarrow \ell^\pm \nu_\ell \ell^+ \ell^-$ for 10 fb^{-1} at the LHC; $280 < M_{WZ} < 340 \text{ GeV}$; other cuts are listed in the text. The color code is given in Fig. 1.

data over the same $\cos \theta$ range, 0.0–0.9, as in Case A. The luminosities of 40 and 80 fb^{-1} were chosen to give roughly the same statistics. For the higher luminosities, the effects of pile-up on

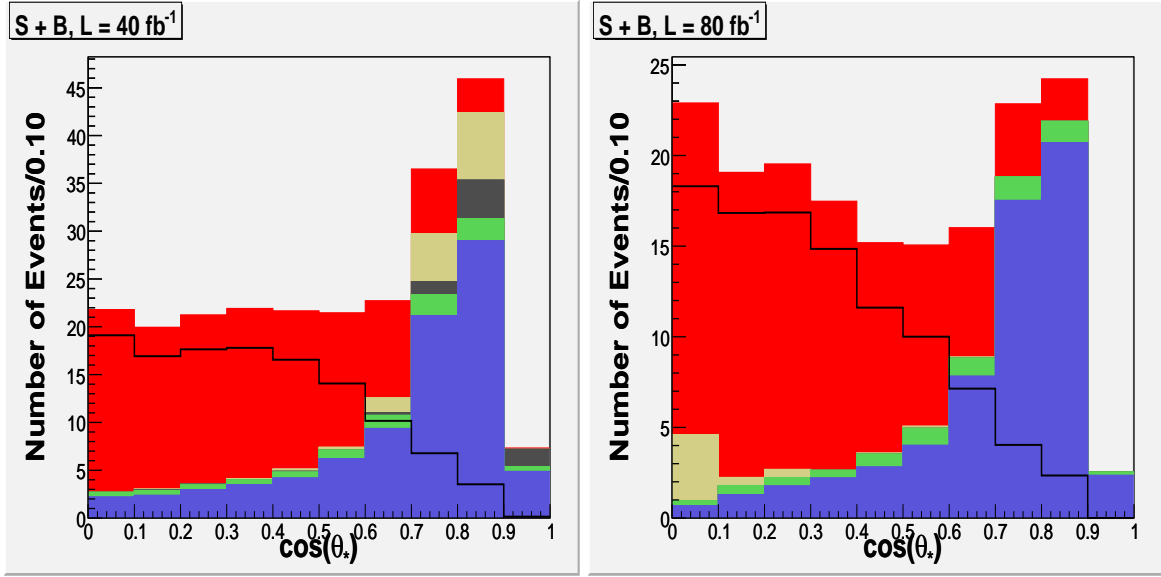


Fig. 3: WZ angular distributions of the signal and backgrounds for $\rho_T^\pm \rightarrow W^\pm Z^0 \rightarrow \ell^\pm \nu_\ell \ell^+ \ell^-$. Left: $M_{\rho_T} = 400$ GeV with $380 < M_{WZ} < 440$ GeV for 40 fb^{-1} . Right: $M_{\rho_T} = 500$ GeV with $480 < M_{WZ} < 540$ GeV for 80 fb^{-1} . Other cuts are listed in the text. The color code is given in Fig. 1.

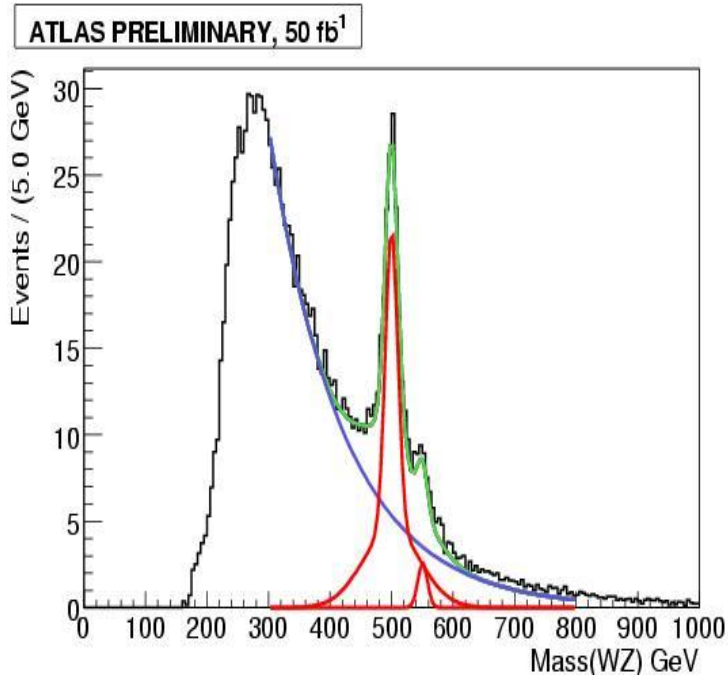


Fig. 4: Fit of the signal and background WZ invariant mass distribution, for case C with 50 fb^{-1} , in ATLAS. Red curves represent the signal resonances, blue the backgrounds, and green the total [44].

calorimetry and tracking were not considered.

Finally, for the 50 GeV splitting used in case C, it appears possible to see ρ_T^\pm and a_T^\pm as separate peaks in the M_{WZ} distribution. This was studied in Refs. [44, 45]. With cuts similar to

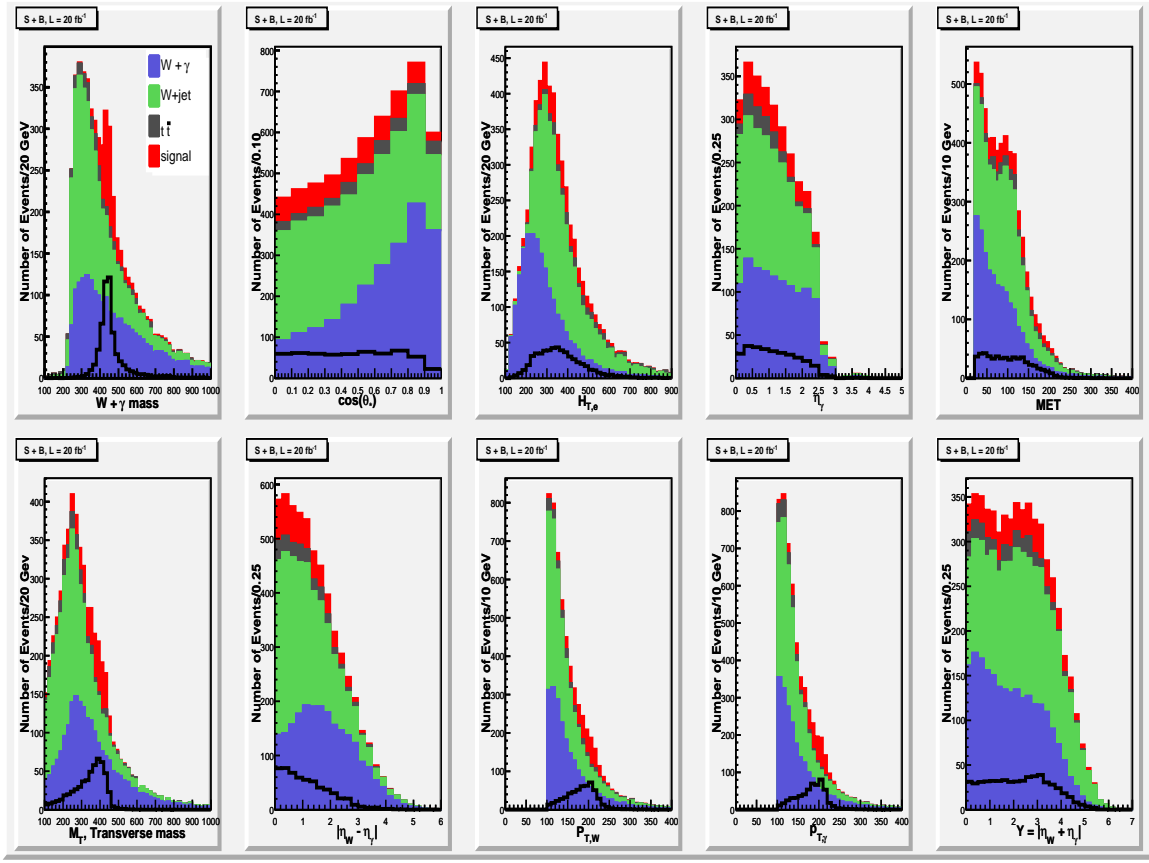


Fig. 5: Signal and background distributions of a 440 GeV $a_T^\pm \rightarrow \gamma W^\pm \rightarrow \gamma \ell^\pm \nu_\ell$ for 20 fb^{-1} at the LHC; $p_T(\gamma, W) > 100 \text{ GeV}$ and $\cancel{E}_T > 20 \text{ GeV}$. The open black histograms are the signal contributions.

those used above (except that $p_T(W, Z) > 50 \text{ GeV}$) a simulation [44] using ATLFAST was performed. The result is in Fig. 4 where a luminosity of 50 fb^{-1} was assumed. The ρ_T and a_T were modeled as Gaussian distributions and the background above 300 GeV as a falling exponential. The a_T appears as a high-mass shoulder. The CMS analysis finds a similar result [45]. Both ρ_T and a_T can be observed and a 5σ (combined) discovery achieved with luminosity $\simeq 9.5 \text{ fb}^{-1}$ provided that data is reasonably described by the simulated \cancel{E}_T resolution.

3. $a_T^\pm \rightarrow \gamma W_L^\pm$

The axial-vector isovector a_T is a new addition to the TCSM framework, motivated by the arguments that the S parameter problem of technicolor is ameliorated if ρ_T and a_T are nearly degenerate and have nearly the same couplings to the vector and axial-vector weak currents.

On account of space limitation, we show here only the results of PGS simulation of Case B, for which $M_{a_T} = 440 \text{ GeV}$. For the decays to a pair of electroweak bosons considered in this report, $\sigma(a_T \rightarrow \gamma W)B(W \rightarrow e/\mu\nu)$ are the largest; it is 65 fb in case B. Signal and background events were generated with $p_T(\gamma) > 40 \text{ GeV}$. As noted, the discovery search could impose a higher threshold. Events were selected with exactly one lepton, having $p_T > 10 \text{ GeV}$ and $|\eta| < 2.5$. Distributions are displayed in Fig. 5, in which $\cancel{E}_T > 20 \text{ GeV}$ and $p_T(\gamma), p_T(W) > 100 \text{ GeV}$. The principal backgrounds are in Table 3. A $\text{jet} \rightarrow \gamma$ fake rate of 10^{-3} was assumed for $W + \text{jet}$ [46]. Another possible background, $\gamma + \text{jet}$ where the

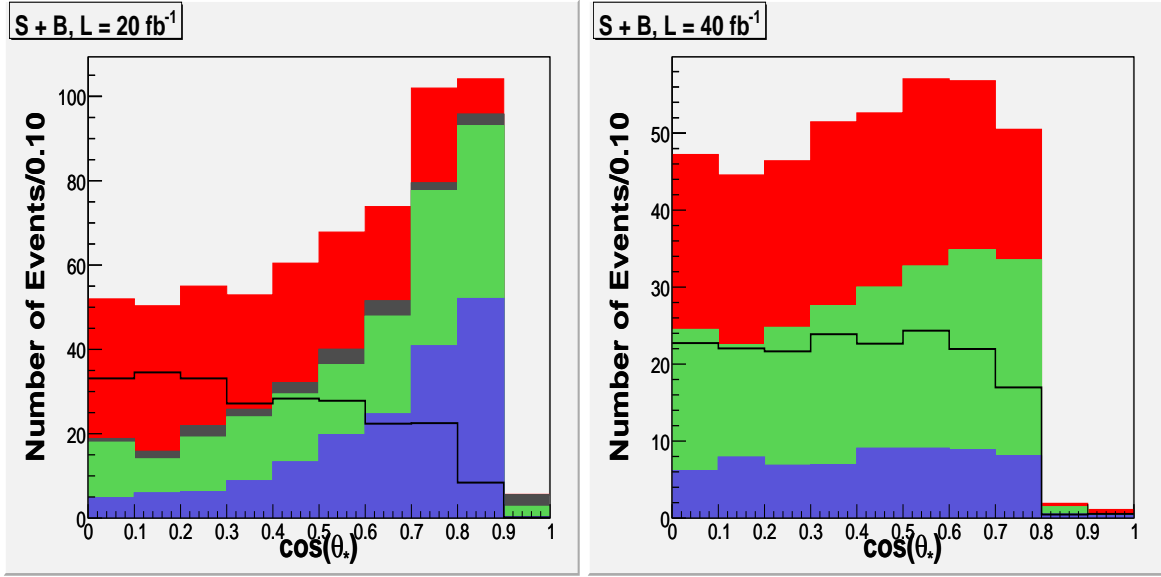


Fig. 6: Angular distributions for the signal and backgrounds for a 440 GeV $a_T^\pm \rightarrow \gamma W^\pm$ with $420 < M_{\gamma W} < 460$ GeV (left) and a 300 GeV $\omega_T \rightarrow \gamma Z^0$ with $290 < M_{\gamma Z} < 310$ GeV (right) at the LHC; other cuts are listed in the text. The luminosities are 20 and 40 fb^{-1} , respectively. The color codes are given in Figs. 5 and 7.

jet fakes a lepton, is negligible after the \cancel{E}_T cut. The luminosity of 20 fb^{-1} was chosen to give reasonable statistics for the signal's angular distribution. Consequently, the a_T resonant peak has a significance of 10σ .

It is clear from these distributions that the backgrounds are a more severe impediment to observing the signal's angular distribution ($1 + \cos^2 \theta$) than they were in the case of $\rho_T \rightarrow WZ$. In particular, there is no obvious cut to remove them other than one on $M_{\gamma W}$. The result of requiring $420 < M_{\gamma W} < 460$ GeV is in Fig. 6. Even though the signal's expected forward-backward excesses are eliminated by the $p_T(\gamma)$ cut, this clearly is a flatter distribution than the $\sin^2 \theta$ ones above. As in that case, subtracting the background by measuring the sidebands should reveal the signal. Careful fitting to see that it is consistent with $1 + \cos^2 \theta$ after cuts is work for the future.

4. $\omega_T \rightarrow \gamma Z_L^0$

The ω_T is as important to find as the ρ_T , with which it is expected to be nearly degenerate, and the a_T . Yet it is the most challenging to see of the light techni-vectors. At the Tevatron, the primary discovery mode is $\omega_T \rightarrow \gamma \pi_T^0 \rightarrow \gamma b\bar{b}$. Backgrounds to this may make this channel difficult at the LHC; studies need to be done! Two other channels have much lower branching ratios, but are much cleaner: $\omega_T \rightarrow \gamma Z_L^0 \rightarrow \gamma \ell^+ \ell^-$ and $\omega_T \rightarrow \ell^+ \ell^-$. We discuss the first of these in this section.¹²

As with the a_T search just described, the main backgrounds to $\omega_T \rightarrow \gamma Z^0$ are standard $Z^0 + \gamma$ and $Z + \text{jet}(\rightarrow \gamma)$ production. The ω_T signal, however, is about 10 times smaller than the a_T one (see Table 2), so considerably higher luminosities are required to see a significant signal peak and the characteristic $1 + \cos^2 \theta$ distribution. Here we discuss the PGS simulation for

¹²Preliminary studies of $\omega_T \rightarrow \mu^+ \mu^-$, including its angular distribution have been carried out by J. Butler and K. Black. The $\omega_T \rightarrow e^+ e^-$ mode is ripe for picking.

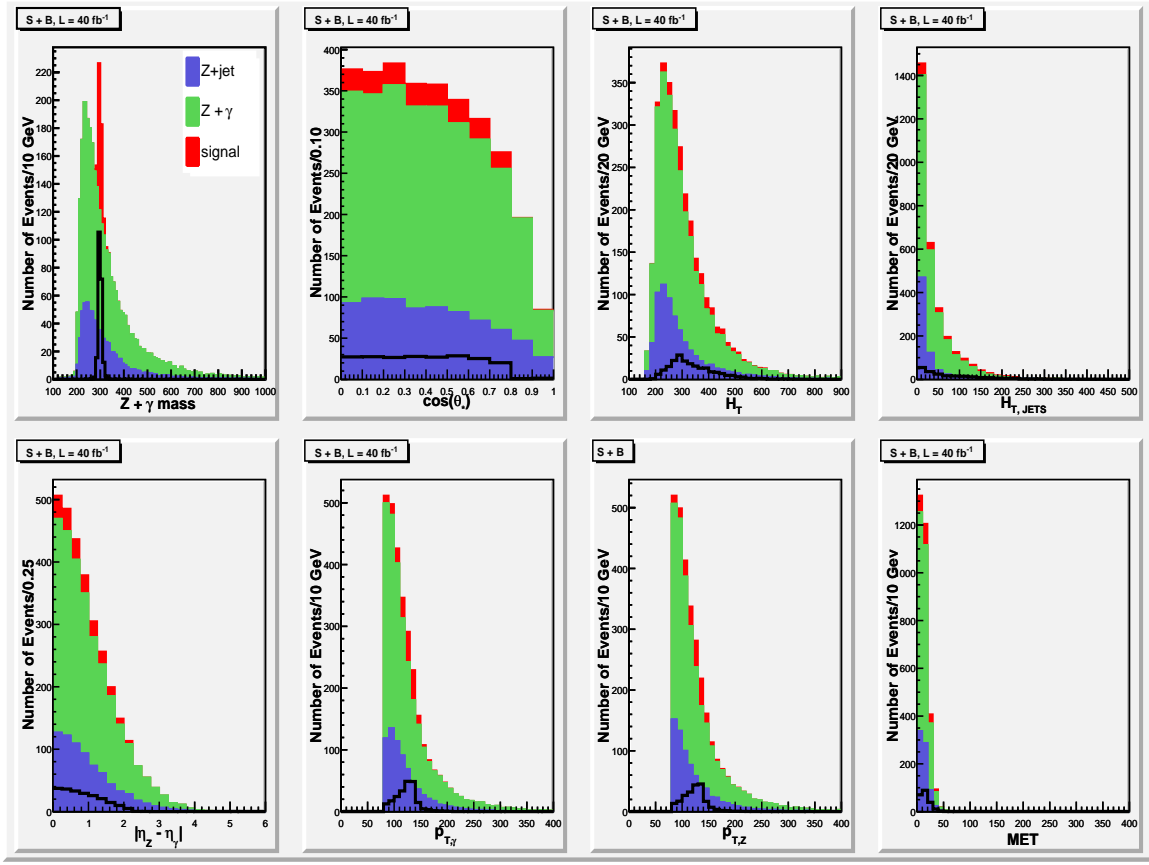


Fig. 7: Signal and background distributions of a 300 GeV $\omega_T \rightarrow \gamma Z^0 \rightarrow \gamma \ell^+ \ell^-$ for 40 fb^{-1} at the LHC; $|M_{\ell^+ \ell^-} - M_Z| < 7.8 \text{ GeV}$ and $p_T(\gamma, Z) > 80 \text{ GeV}$. The open black histograms are the signal contributions.

case A, in which $M_{\omega_T} = 300 \text{ GeV}$. Events were selected with two same-flavor, opposite-sign leptons, each having $p_T > 10 \text{ GeV}$ and rapidity $|\eta| < 2.5$. The leptons were required to satisfy $|M_{\ell^+ \ell^-} - M_Z| < 7.8 \text{ GeV}$. Distributions are shown in Fig. 7 for a luminosity of 40 fb^{-1} and for $p_T(\gamma), p_T(Z) > 80 \text{ GeV}$. Note the much better final-state mass resolution than for $\rho_T \rightarrow WZ$ and $a_T \rightarrow \gamma W$. The significance of the signal peak is about 8σ ; the high luminosity is needed to accumulate statistics for the angular distribution.¹³

To expose the angular distribution, we take advantage of the superior γZ mass resolution and impose a tight cut on $M_{\gamma Z}$ of $300 \pm 10 \text{ GeV}$. The result is in Fig. 6. Because of the more stringent p_T cuts, the data above $|\cos \theta| > 0.8$ are lost. While quite acceptable, the angular distribution's signal-to-background is not as favorable as it was for $a_T \rightarrow \gamma W$. As in that case, detailed fitting beyond our scope is needed to determine how well the measured distribution fits the expectation. And, as there, the backgrounds can be subtracted by measuring the angular distribution in sidebands.

5. $\rho_T^\pm, a_T^\pm \rightarrow Z^0 \pi_T^\pm \rightarrow \ell^+ \ell^- b q$

Even if narrow resonances in the $WZ, \gamma W$ and γZ channels are found as described above at the LHC, all with nearly the same mass and with the expected angular distributions, it will remain

¹³For case B, the corresponding luminosity is 80 fb^{-1} .

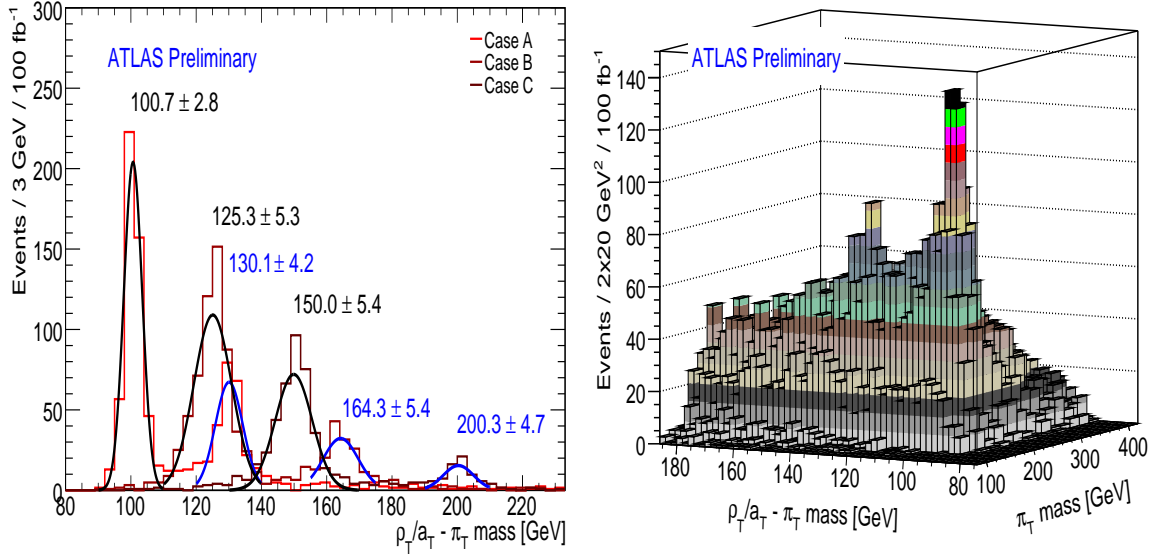


Fig. 8: Left: $M_{\rho_T} - M_{\pi_T}$ and $M_{a_T} - M_{\pi_T}$ for cases A, B, C in ATLAS. Right: $M_{\rho_T, a_T} - M_{\pi_T}$ vs. M_{π_T} signal and background events per $2 \times 10 \text{ GeV}^2$ per 100 fb^{-1} for case A [39].

essential to discover a technipion to cement the technicolor interpretation of these states. In this section we present an analysis of $\rho_T^\pm \rightarrow Z^0 \pi_T^\pm$ carried out for the ATLAS detector [39]. The large backgrounds to this signal require large luminosity. On the other hand, for the masses assumed here, this channel has the extra advantage that the rate for $a_T^\pm \rightarrow Z^0 \pi_T^\pm$ is only about 2–4 times smaller than for $\rho_T^\pm \rightarrow Z^0 \pi_T^\pm$, creating another opportunity for observing both resonant peaks in the same (well, similar) final state.

As noted, π_T are expected to decay into the heaviest fermion-antifermion flavors kinematically allowed. For the range of M_{π_T} considered here, this implies $\pi_T^+ \rightarrow t\bar{b}$ and $\pi_T^- \rightarrow b\bar{t}$ or $t\bar{t}$ are dominant. Actually, something like topcolor-assisted technicolor [29] is needed to produce $m_t \simeq 175 \text{ GeV}$, and this implies that the coupling of π_T to t -quarks is suppressed by a factor of about m_b/m_t from its naive value. Thus, while the π_T^+ considered here is massive enough to decay to $t\bar{q}$, it should still have an appreciable branching fraction to $c\bar{b}$ and $u\bar{b}$. The latter are the decay channels considered here. It will be interesting to consider the $t\bar{q}$ modes. However, they are not yet included in PYTHIA and, therefore, $B(\pi_T^+ \rightarrow b\bar{q}) = 0.87$ in the simulation reported here. This branching ratio may decrease substantially when the top modes are included. That would change the search strategy, but we expect that π_T^+ can be seen in $t\bar{q}$ as well.

The signal cross sections are $\sigma(pp \rightarrow \rho_T^\pm, a_T^\pm \rightarrow Z^0 \pi_T^\pm) B(Z^0 \rightarrow \ell^+ \ell^-) = (99, 59)$ (A), (71, 17) (B), and (37, 9) fb (C), where the two numbers are approximately the ρ_T^\pm and a_T^\pm contributions. The principal backgrounds and their leading-order cross sections are: $t\bar{t}$ (500 pb) and, including the branching ratio of Z^0 to e^+e^- and $\mu^+\mu^-$, $Z^0 jj$ (344 pb), $Z^0 b\bar{b}$ (56 pb) and $Z^0 bj$ (11 pb).¹⁴ See Ref. [39] for generation details. The ATLAS detector simulation used ATLAS-FAST [38]. An additional factor of 90% was applied to the simulation for lepton identification

¹⁴Recall footnote 8 regarding systematic errors on such backgrounds. Background contributions from processes with even more jets are possible; they are partly accounted for by the leading-log parton showering approximation and initial and final state QCD radiation in Pythia. The $Z^0 b\bar{b}$ rate here is much larger than in Table 3 because it was generated with greater b -jet acceptance.

efficiency. The b -jet tag efficiency used was 60% with corresponding global mistagging factors of $\sim 1\%$ for light-quark and gluon jets and $\sim 10\%$ for c -jets. The exact rejection factors depend on the reconstructed jet p_T and η .

To satisfy ATLAS trigger and high-luminosity (100 fb^{-1} per year) running conditions, events were preselected with (1) two same-flavor opposite-sign leptons with $p_T > 20 \text{ GeV}$ and (2) at least one b -tagged jet and one non- b -tagged jet, both with $p_T > 20 \text{ GeV}$; the two highest- p_T jets satisfying these conditions are the π_T -candidate jets. For the ρ_T^\pm , these selections resulted in 548 (A), 382 (B) and 184 (C) signal events per 100 fb^{-1} . For the a_T^\pm , there were 297 (A), 117 (B) and 34 (C) events. The total background event numbers, dominated by Zjj and $Zb\bar{b}$, were: (6930, 10670) (A), (7505, 6285) (B) and (3015, 2550) (C). Here, the first number in each pair refers to ρ_T and the second to a_T ; the background is the number of events in an elliptical region in $M_{\pi_T} - (M_{\rho_T, a_T} - M_{\pi_T})$ space centered at the mean and with widths corresponding to 1.5σ .

The following cuts were then applied to optimize the signal significances: (1) $\cancel{E}_T < 35 \text{ GeV}$ to suppress $t\bar{t}$; (2) the highest- p_T jet had $p_T > 80$ (A), 115 (B), 150 GeV (C); (3) the second highest- p_T jet had $p_T > 65$ (A), 80 (B), 100 GeV (C); (4) there is exactly one b -tagged jet; and (5) $M_{\ell+\ell^-} = 91 \pm 5 \text{ GeV}$. After these cuts, the number of remaining signal events is (344, 215) (A), (242, 75) (B) and (126, 21) (C) for (ρ_T^\pm, a_T^\pm) . The backgrounds under these signals are (403, 900) (A), (346, 242) (B) and (96, 69) (C). For the parameters used in this simulation, then, only in case C is the a_T not observable in the $Z\pi_T$ channel in 100 fb^{-1} .

The resolution in M_{π_T} varies from 16 to 23 GeV and in M_{ρ_T, a_T} from 19 to 30 GeV. Most of the error comes from the π_T jets' energy measurements. Therefore, much of it cancels in $Q = M_{\rho_T, a_T} - M_{\pi_T}$. This is shown on the left in Fig. 8, where the resolution in this difference ranges from 3 to 5 GeV. This sharpness will facilitate the discovery of $\rho_T, a_T \rightarrow Z\pi_T$ and other technivector-to-technipion decays.¹⁵ The signals and background for case A are on the right in Fig. 8. The twin peaks stand out dramatically (looking rather like Boston's Back Bay).

In summary: For the TCSM parameters used here, there should be no difficulty seeing ρ_T^\pm and a_T^\pm in the $Z^0\pi_T^\pm$ channel in case A, and the ρ_T and a strong indication of the a_T in case B. In case C, only $\rho_T^\pm \rightarrow Z^0\pi_T^\pm$ can be seen in 100 fb^{-1} . The minimal cross sections (times $B(Z \rightarrow e^+e^- / \mu^+\mu^-)$) and luminosities required to see the ρ_T^\pm and a_T^\pm signals at 5σ significance are in Table 5.

peak	A	B	C		A	B	C
ρ_T^\pm	29	28	14		8.3	15	15
a_T^\pm	41	18	18		48	106	390

Table 5: Minimal cross-section times branching fractions (in fb, left) and minimal luminosities (in fb^{-1} , right) required for 5σ significance in cases A, B, C.

¹⁵The Q -value was used to advantage in the most recent CDF search for $\rho_T \rightarrow W^\pm\pi_T \rightarrow \ell^\pm\nu_\ell b\text{jet}$; see CDF/ANAL/EXOTIC/PUBLIC/8566, <http://www-cdf.fnal.gov/physics/exotic/r2a/20061025.techcolor/>, and its importance was emphasized in Ref. [26].

6. CONCLUSIONS AND OUTLOOK

Low-scale technicolor (with $N_D = \mathcal{O}(10)$ isodoublets transforming as $SU(N_{TC})$ fundamentals) is a well-motivated scenario for strong electroweak symmetry breaking with a walking TC gauge coupling. The Technicolor Straw-Man framework provides the simplest phenomenology of this scenario by assuming that the lightest technihadrons — ρ_T , ω_T , a_T and π_T — and the electroweak gauge bosons can be treated in isolation. This framework is now implemented in PYTHIA.

We used PYTHIA and (mainly) the generic detector simulator PGS to study the final-state mass peaks and angular distributions for the LSTC discovery channels at the LHC: $\rho_T^\pm \rightarrow W^\pm Z^0$, $a_T^\pm \rightarrow \gamma W^\pm$ and $\omega_T \rightarrow \gamma Z^0$, with leptonic decays of the weak bosons. We also carried out an ATLFASST simulation for ρ_T^\pm , $a_T^\pm \rightarrow Z^0 \pi_T^\pm \rightarrow \ell^+ \ell^- b \text{ jet}$. The results are very promising. For the fairly generic TCSM parameters chosen, the technivector mesons can be discovered up to about 500–600 GeV in the two-gauge boson modes, usually with a few to a few tens of fb^{-1} . The angular distributions, dispositive of the underlying technicolor dynamics, can be discerned with a few tens to 100 fb^{-1} (except for a higher mass $\omega_T \rightarrow \gamma Z^0$). Taking advantage of the superb resolutions in $Q = M_{\rho_T, a_T} - M_{\pi_T}$ and $M_{\ell^+ \ell^-}$ for ρ_T , $a_T \rightarrow Z \pi_T \rightarrow \ell^+ \ell^- b \text{ jet}$, both resonances and the technipion can be seen for $M_{\rho_T} \lesssim 500 \text{ GeV}$ and $M_{a_T} \lesssim 400 \text{ GeV}$.

Still, these studies just scratch the surface of what can and needs to be done to gauge the potential of the ATLAS and CMS detectors for discovering and probing low-scale technicolor. Simulating detector response to the signals and backgrounds of the relatively simple processes we considered requires considerably more sophistication, in both depth and breadth, than we have been able to deploy. Issues such as the accuracy with which technivector masses and decay angular distributions can be determined as a function of luminosity are especially important. While we believe that the TCSM parameters — $\sin \chi$, $Q_U + Q_D$, M_{π_T} , M_{V_i} and M_{A_i} , N_{TC} — we chose are reasonable, relative branching fractions can be fairly sensitive to them, as Table 1 indicates [28]. It would be valuable to reconsider the processes examined here for a range of these parameters. Finally, there are other modes we have not been able to consider but which are nevertheless of considerable interest. Two outstanding examples are ρ_T^0 , ω_T , $a_T^0 \rightarrow \ell^+ \ell^-$ and ω_T , $\rho_T^0 \rightarrow \gamma \pi_T^0 \rightarrow \gamma \bar{b} b$. Thus, the main goal of our Les Houches studies, as it is for the other “Beyond the Standard Model” ones started at Les Houches, is to motivate the ATLAS and CMS collaborations to broaden the scope of their searches for the origin and dynamics of electroweak symmetry breaking.

“Faith” is a fine invention
 When Gentlemen can see —
 But *Microscopes* are prudent
 In an Emergency.

— Emily Dickinson, 1860

Acknowledgments

We thank the organizers and conveners of the Les Houches workshop, “Physics at TeV Colliders”, for a most stimulating meeting and for their encouragement in preparing this work. We are especially grateful to Steve Mrenna for updating PYTHIA to include all the new TCSM pro-

cesses. We also thank participants, too many to name, for many spirited discussions. Lane and Martin are indebted to Laboratoire d'Annecy-le-Vieux de Physique des Particules (LAPP) and Laboratoire d'Annecy-le-Vieux de Physique Theorique (LAPTH) for generous hospitality and support throughout the course of this work. Part of this work has been performed within the ATLAS Collaboration (Azuelos and Ferland; Black) and the CMS Collaboration (Bose), and we thank members of both collaboration for helpful discussions. We have made use of their physics analysis framework and tools which are the result of collaboration-wide efforts. This research was supported in part by NSERC, Canada (Azuelos and Ferland) and the U.S. Department of Energy under Grants DE-FG02-91ER40654 (Black), DE-FG02-91ER40688 (Bose), DE-FG02-97ER41022 (Gershtein), DE-FG02-91ER40676 (Lane), and DE-FG02-92ER40704 (Martin).

References

- [1] S. Weinberg, *Phys. Rev.* **D19** (1979) 1277–1280.
- [2] L. Susskind, *Phys. Rev.* **D20** (1979) 2619–2625.
- [3] B. Holdom, *Phys. Rev.* **D24** (1981) 1441.
- [4] T. W. Appelquist, D. Karabali, and L. C. R. Wijewardhana, *Phys. Rev. Lett.* **57** (1986) 957.
- [5] K. Yamawaki, M. Bando, and K.-i. Matumoto, *Phys. Rev. Lett.* **56** (1986) 1335.
- [6] T. Akiba and T. Yanagida, *Phys. Lett.* **B169** (1986) 432.
- [7] E. Eichten and K. D. Lane, *Phys. Lett.* **B90** (1980) 125–130.
- [8] K. Lane, hep-ph/0202255.
- [9] C. T. Hill and E. H. Simmons, *Physics Reports* **381** (2003) 235–402, [hep-ph/0203079].
- [10] K. D. Lane and E. Eichten, *Phys. Lett.* **B222** (1989) 274.
- [11] E. Eichten and K. D. Lane, *Phys. Lett.* **B388** (1996) 803–807, [hep-ph/9607213].
- [12] E. Eichten, K. D. Lane, and J. Womersley, *Phys. Lett.* **B405** (1997) 305–311, [hep-ph/9704455].
- [13] E. Eichten, I. Hinchliffe, K. D. Lane, and C. Quigg, *Rev. Mod. Phys.* **56** (1984) 579–707.
- [14] T. Appelquist and R. Shrock, *Phys. Lett.* **B548** (2002) 204–214, [hep-ph/0204141].
- [15] T. Appelquist, M. Piai, and R. Shrock, *Phys. Rev.* **D69** (2004) 015002, [hep-ph/0308061].
- [16] K. D. Lane, hep-ph/9401324.
- [17] K. D. Lane, hep-ph/9409304.
- [18] M. E. Peskin and T. Takeuchi, *Phys. Rev. Lett.* **65** (1990) 964–967.
- [19] M. Golden and L. Randall, *Nucl. Phys.* **B361** (1991) 3–23.
- [20] B. Holdom and J. Terning, *Phys. Lett.* **B247** (1990) 88–92.
- [21] G. Altarelli, R. Barbieri, and S. Jadach, *Nucl. Phys.* **B369** (1992) 3–32.
- [22] T. Appelquist and F. Sannino, *Phys. Rev.* **D59** (1999) 067702, [hep-ph/9806409].
- [23] M. Knecht and E. de Rafael, *Phys. Lett.* **B424** (1998) 335–342, [hep-ph/9712457].
- [24] J. Hirn and V. Sanz, *Phys. Rev. Lett.* **97** (2006) 121803, [hep-ph/0606086].
- [25] J. Hirn and V. Sanz, hep-ph/0612239.

- [26] E. Eichten and K. Lane, arXiv:0706.2339 [hep-ph].
- [27] K. D. Lane, *Phys. Rev.* **D60** (1999) 075007, [hep-ph/9903369].
- [28] K. Lane and S. Mrenna, *Phys. Rev.* **D67** (2003) 115011, [hep-ph/0210299].
- [29] C. T. Hill, *Phys. Lett.* **B345** (1995) 483–489, [hep-ph/9411426].
- [30] P. Kreuzer, *Acta Phys. Polon.* **B38** (2007) 459–468.
- [31] “Pgs - pretty good simulator.”
<http://www.physics.ucdavis.edu/conway/research/software/pgs/pgs4-general.htm>.
- [32] R. Sekhar Chivukula, E. H. Simmons, H.-J. He, M. Kurachi, and M. Tanabashi, *Phys. Rev.* **D71** (2005) 035007, [hep-ph/0410154].
- [33] R. S. Chivukula, E. H. Simmons, H.-J. He, M. Kurachi, and M. Tanabashi, *Phys. Rev.* **D71** (2005) 115001, [hep-ph/0502162].
- [34] C. Csaki, C. Grojean, H. Murayama, L. Pilo, and J. Terning, *Phys. Rev.* **D69** (2004) 055006, [hep-ph/0305237].
- [35] C. Csaki, C. Grojean, L. Pilo, and J. Terning, *Phys. Rev. Lett.* **92** (2004) 101802, [hep-ph/0308038].
- [36] K. Agashe, A. Delgado, M. J. May, and R. Sundrum, *JHEP* **08** (2003) 050, [hep-ph/0308036].
- [37] G. Cacciapaglia, C. Csaki, C. Grojean, and J. Terning, *Phys. Rev.* **D71** (2005) 035015, [hep-ph/0409126].
- [38] E. Richter-Was, D. Froidevaux, and L. Poggioli, “Atlfast.” ATLAS Note, ATL-PHYS-98-131, <http://www.hep.ucl.ac.uk/atlas/atlfast/UserGuide.html>, 1998.
- [39] G. Azuelos, J. Ferland, K. Lane, and A. Martin, “Search for low-scale technicolor in atlas.” ATLAS Note, ATL-PHYS-CONF-2008-003, 2008.
- [40] T. Sjostrand, S. Mrenna, and P. Skands, *JHEP* **05** (2006) 026, [hep-ph/0603175].
- [41] F. Maltoni and T. Stelzer, *JHEP* **02** (2003) 027, [hep-ph/0208156].
- [42] J. Alwall *et. al.*, *JHEP* **09** (2007) 028, [arXiv:0706.2334 [hep-ph]].
- [43] M. L. Mangano, M. Moretti, F. Piccinini, R. Pittau, and A. D. Polosa, *JHEP* **07** (2003) 001, [hep-ph/0206293].
- [44] K. Black, “Searches for technicolor in the trilepton final state.” ATLAS Note, ATL-PHYS-CONF-2008-004, 2008.
- [45] T. Bose, “A search for technicolor in the tri-lepton final state.” CMS Note, CMS CR-2008/004.
- [46] “Atlas detector and physics performance. technical design report. vol. 2.” CERN-LHCC-99-15.